IEEE POWER ELECTRONICS REGULAR PAPER

Online MTPA Operation of IPMSM based on Dual-Loop Control in Polar Coordinates

Hyeon-Sik Kim, *Member, IEEE*, Jiwon Yoo, *Student Member, IEEE*, and Seung-Ki Sul, *Fellow, IEEE*

***Abstract*— In this paper, a maximum online torque per ampere (MTPA) control is proposed for torque control of interior permanent magnet synchronous motors (IPMSMs). First, torque and MTPA equations are derived based on flux variables, where the influence of magnetic saturation and cross-coupling effects is carefully considered. These equations can be described in polar coordinates, in which the output torque and MTPA operation are mainly determined by the current magnitude and current angle, respectively. Consequently, a dual-loop controller is proposed to solve the torque and MTPA equations in polar coordinates with a lower computational burden. It consists of a current magnitude and a current angle controller, where a torque reference limiter is embedded to satisfy the current limit. Moreover, the current angle is set within a stable range to avoid the stuck of the controller. The effectiveness of the proposed method is verified through simulation and experimental results. Applying the proposed algorithms, both MTPA operation and torque accuracy can be achieved with less computational burden.**

***Index Terms*—IPMSM, loss minimization, maximum torque per ampere (MTPA), minimum copper-loss operation, torque control, polar coordinates.**

I. INTRODUCTION

For interior permanent magnet synchronous motor (IPMSM) drives, accurate torque control and loss-minimizing operation are essential issues for maintaining their excellent features such as high power density and high efficiency. Thus, the current magnitude should be minimized while maintaining the torque accuracy under the base speed in the maximum torque per ampere (MTPA) region. To achieve MTPA operation, the current angle and current magnitude should be accurately adjusted to utilize both the field torque from the permanent magnet and the reluctance torque from the difference in reluctance. In addition, the current magnitude should be limited to a specific limit to satisfy thermal and instantaneous current constraints of the inverter and motor itself. However, nonlinear characteristics such as magnetic saturation and cross-coupling effects make it difficult to satisfy both MTPA operation and torque accuracy under current and voltage constraints [1].

Mostly, look-up table (LUT) methods have been adopted for the torque control of an IPMSM to prevent complicated calculations in real-time [2], [3]. However, offline-calculated LUTs should be built through costly and time-consuming processes. Sometimes, linear equations have been derived to replace LUTs by applying the curve fitting method, which is also largely dependent on pretest results [4], [5]. Moreover, temperature variation and manufacturing tolerance could provoke flux linkage variations, which would result in torque errors. Thus, various online MTPA control algorithms have been extensively studied to overcome these issues.

First, perturbation and searching methods had been proposed in which the MTPA condition could be maintained under the variation of machine parameters [6]–[8]. They utilized flux linkage variations by tracing the fluctuation of the output torque [6], output power [7], or current vector [8] after injecting a current angle perturbation. However, these methods can only be used for speed-control applications, where a feedback control loop controls the speed. Thus, torque accuracy cannot be guaranteed in torque-control applications such as traction motor drives in the automotive industry. Moreover, the dynamic performance of the searching method is too slow to be applied to rapid changes in the torque reference.

Alternatively, several adaptive torque control methods have been developed, in which the torque reference can be tracked by a closed-loop torque controller [9], [10]. The accuracy of these methods is highly dependent on the estimation performance of the *d*- and *q*- axis static inductances and the magnet flux linkage, i.e., L_{ds}, L_{qs}, and λ_f. However, it has been well known that simultaneous estimation of both the *q*-axis static inductance and magnetic flux linkage with reasonable accuracy is quite difficult owing to the rank deficiency of the IPMSM's electrical model [11]. Moreover, an MTPA equation has been derived without taking account of inductance variations about currents. The *d*- and *q*- axis static inductances are assumed to be piecewise constant, i.e., $\partial L_{ds}/\partial i_d = \partial L_{qs}/\partial i_q = 0$. This would cause an MTPA tracking error under heavily saturated conditions due to the nonlinear characteristics of the IPMSM [12].

However, some calculation methods have been proposed based on the mathematical model of the IPMSM. In these methods, the torque and MTPA equations were derived using the Lagrange method. These equations can be solved using either analytical or numerical approaches [13]–[15]. They can provide fast dynamic performance and torque accuracy by updating the motor parameters in real-time. However, these methods suffer from high computational burdens due to complex calculations, e.g., Ferrari's method [13]. In addition, the risk of ill-convergence increases under highly saturated

Hyeon-Sik Kim is with the Department of Electrical Engineering, Gachon University, Seongnam 13120, Korea (e-mail: hyeonsik@gachon.ac.kr).

Jiwon Yoo and Seung-Ki Sul are with the Department of Electrical and Computer Engineering, Seoul National University, Seoul, 08826, Korea (e-mail: jiwon.yoo@eepel.snu.ac.kr; sulsk@plaza.snu.ac.kr).

conditions when using a numerical approach, e.g., Newton's method [14]. The Levenberg–Marquardt method was recently utilized to improve the robustness of online MTPA control while minimizing the calculation burden [15]. Nevertheless, these methods cannot be easily implemented with a low-cost digital signal processor (DSP) owing to the calculation loads.

Furthermore, the torque and MTPA equations have been defined as the function of the stator flux magnitude and the load angle [16], [17]. The direct flux vector control (DFVC) was adopted to track both the torque reference and MTPA trajectory based on auxiliary-flux and auxiliary-current vectors. The optimal references for the DFVC scheme were calculated from a small-signal model around the operating point.

In summary, conventional methods have both advantages and disadvantages regarding accuracy, dynamics, and calculation burden. Compared with other methods, the calculation methods based on a mathematical model are advantageous in terms of dynamics. In addition, the torque accuracy and efficiency can be further enhanced by simultaneously applying online parameter estimation algorithms [18]. However, the complexity of their implementation could be an obstacle to practical applications. This makes it challenging to reflect the variation in constraints and optimize the performance of the calculation algorithms in real-time. Thus, if the calculation algorithm is simplified while maintaining sufficient steady-state and dynamic performances, the algorithm's applicability can be significantly extended.

In this paper, a closed-loop torque and MTPA controller are proposed to achieve the online MTPA operation of an IPMSM with a more straightforward implementation. This method is called dual-loop control. It consists of a current magnitude and current angle controller in polar coordinates, where the closed dual-loop control solves the torque and MTPA equations. It can provide satisfactory dynamic performance and torque accuracy by reflecting the IPMSM parameters, such as flux linkages and dynamic inductances, in real-time.

Moreover, a torque reference limiter is embedded in the proposed current magnitude controller to restrict the magnitude of the current references under high-torque commands. The output of the current angle controller is limited to suppressing the stuck on the wrong operating points. The calculation burden can be remarkably reduced because of the closed-loop structure compared to conventional calculation methods. Finally, simulation and experimental results are provided to verify the validity of the proposed method. The contents of this research, previously presented in [19], have been largely revised to understand better. The contributions of this paper are summarized as follows:

1) The torque and MTPA equations are derived in polar coordinates. This reveals that flux linkages at the operating point and its variations in θ coordinate are required for the online MTPA operation.
2) The dual-loop controller is proposed to trace both the torque reference and MTPA trajectory without a premade MTPA LUT. The proposed closed-loop structure is analyzed in terms of stability and dynamics, where the nonlinear characteristics of the IPMSM are considered.
3) The adequate flux linkage LUTs and estimation algorithms are discussed to update IPMSM parameters in the proposed controller.

TABLE I
NOMINAL IPMSM PARAMETERS

Parameter	Value
Number of pole pairs, P	4
Maximum power, P_{max}	45 kW
Maximum torque, $T_{e,max}$	54 N·m
Rated speed, ω_{rated}	8000 r/min
Permanent magnet flux linkage at zero torque, λ_d @ T_e^* = 0 pu	0.43 pu
d-axis flux linkage at max. torque, λ_d @ T_e^* = 1 pu	0.14 pu
q-axis flux linkage at max. torque, λ_q @ T_e^* = 1 pu	0.57 pu

II. IPMSM MODELING

A. Modeling in Cartesian Coordinates

For IPMSM, the flux linkages, (λ_d, λ_q), are usually set as a linear function of stator currents in d-q coordinates, (i_d, i_q), for unsaturated conditions as follows:

$$\begin{cases} \lambda_d(i_d, i_q) = L_{ds} i_d + \lambda_f \\ \lambda_q(i_d, i_q) = L_{qs} i_q \end{cases}, \tag{1}$$

where (L_{ds}, L_{qs}) denote d- and q- axis static inductances and λ_f means a permanent magnet flux linkage.

However, it is challenging to express nonlinear characteristics of the IPMSM under saturated conditions because (L_{ds}, L_{qs}) are set to be piecewise constant. Thus, the flux linkages are defined as a piecewise linear model, which is a small-signal model around the operating point as

$$\begin{cases} \lambda_d(i_d, i_q) = L_{dd}(i_d - i_{do}) + L_{dq}(i_q - i_{qo}) + \lambda_{do}(i_{do}, i_{qo}) \\ \lambda_q(i_d, i_q) = L_{qd}(i_d - i_{do}) + L_{qq}(i_q - i_{qo}) + \lambda_{qo}(i_{do}, i_{qo}) \end{cases}, \tag{2}$$

where (i_{do}, i_{qo}) represent the d- and q- axis currents at the operating point, (L_{dd}, L_{dq}, L_{qd}, L_{qq}) denote the dynamic inductances, and (λ_{do}, λ_{qo}) designate the d- and q- axis flux linkages at (i_{do}, i_{qo}).

The dynamic inductances are the rate of change of the flux linkages relative to the currents at the operating point [20]. The derivative form of (2) is expressed as

$$\begin{cases} \dfrac{d\lambda_d(i_d, i_q)}{dt} = \dfrac{\partial \lambda_d}{\partial i_d}\dfrac{di_d}{dt} + \dfrac{\partial \lambda_d}{\partial i_q}\dfrac{di_q}{dt} = L_{dd}\dfrac{di_d}{dt} + L_{dq}\dfrac{di_q}{dt} \\ \dfrac{d\lambda_q(i_d, i_q)}{dt} = \dfrac{\partial \lambda_q}{\partial i_d}\dfrac{di_d}{dt} + \dfrac{\partial \lambda_q}{\partial i_q}\dfrac{di_q}{dt} = L_{qd}\dfrac{di_d}{dt} + L_{qq}\dfrac{di_q}{dt} \end{cases}, \tag{3}$$

where (L_{dd}, L_{qq}) represent the self-inductances and (L_{dq}, L_{qd}) denote the mutual-inductances between the d- and q- axis.

Fig. 1 shows the flux linkages of a motor under test in d-q coordinates, where the parameters are extracted using finite element analysis (FEA) software. The parameters are presented on a per-unit (pu) basis. The base current is defined as the peak current for a short time, where the maximum torque is defined as 1 pu, as presented in Table I. The maximum power is obtained at the rated speed, which is also defined as 1 pu. In Fig. 1, it can be noticed that the saturation and cross-coupling effects are severe under high-torque references, that is, when $|T_{e\_ref}|$ is

This article has been accepted for publication in a future issue of this journal, but has not been fully edited. Content may change prior to final publication. Citation information: DOI 10.1109/TPEL.2021.3120405, IEEE Transactions on Power Electronics

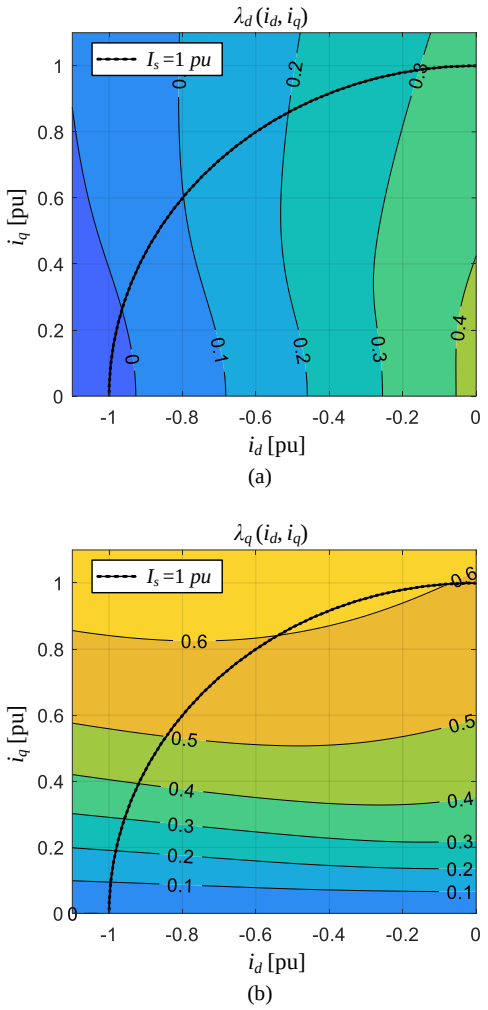

Fig. 1. Flux linkages with *d*-*q* axes. (a) λ_d (i_d, i_q). (b) λ_q (i_d, i_q).

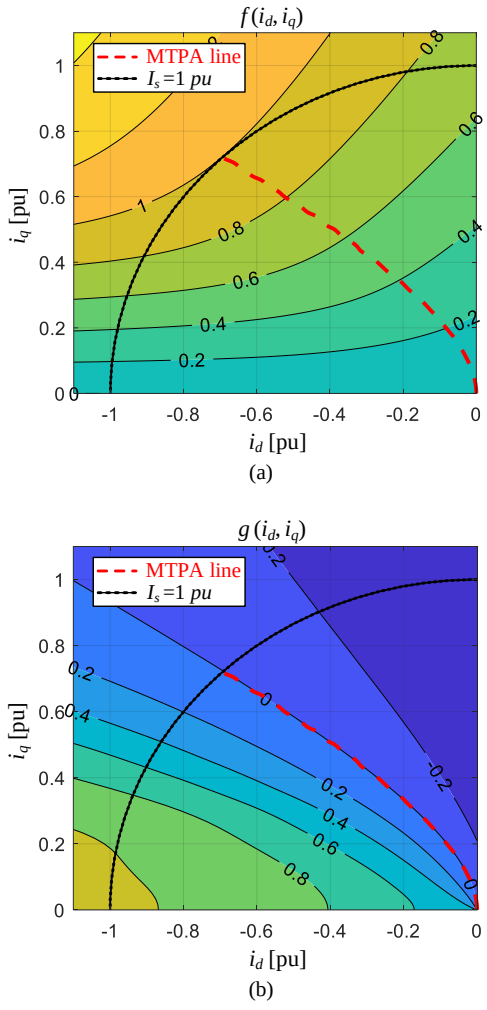

Fig. 2. Contours of torque and MTPA equations with *d*-*q* axes. (a) $f(i_d, i_q)$. (b) $g(i_d, i_q)$.

close to 1 pu. λ_d varies with i_d and i_q, as shown in Fig. 1(a). Likewise, λ_q is a function of i_q and i_d, as shown in Fig. 1(b). It can be modeled as self- and mutual-dynamic inductances.

The electromagnetic torque, T_e, can be defined as the following torque equation, $f(i_d, i_q)$:

$$f(i_d, i_q) = \frac{3P}{2}(\lambda_d i_q - \lambda_q i_d), \tag{4}$$

which is the cross product of flux linkages and stator currents in *d*-*q* coordinates, and P is the number of pole pairs.

Furthermore, the MTPA equation is derived using the Lagrange method [15]. It can be normalized by the current magnitude, i.e., $\sqrt{i_d^2 + i_q^2}$, as follows:

$$g(i_d, i_q) = \frac{1}{\sqrt{i_d^2 + i_q^2}}((L_{qq} i_d^2 - (L_{dq} + L_{qd}) i_d i_q + L_{dd} i_q^2) - (\lambda_d i_d + \lambda_q i_q)) \tag{5}$$

MTPA operation can be achieved when $g(i_d, i_q) = 0$, where the magnetic saturation and cross-coupling effects are fully considered using flux linkages and dynamic inductances.

Fig. 2 shows the contours of $f(i_d, i_q)$ and $g(i_d, i_q)$ for the motor under test in *d*-*q* coordinates based on the per-unit (pu) basis. The red dashed line indicates the MTPA trajectory, which is plotted to trace the minimum distance between a constant torque curve and zero current point. Fig. 2(a) shows that the torque accuracy is achieved when $f(i_d, i_q)$ is equal to the torque reference, $T_{e,ref}$, which is expressed as a constant torque curve. Fig. 2(b) shows that the MTPA operation is satisfied when $g(i_d, i_q)$ is equal to zero, which is identical to the MTPA trajectory.

B. Modeling in Polar Coordinates

Cartesian coordinates can be converted into polar coordinates, i.e., from *d*-*q* to *R*-θ coordinates. The relationship between Cartesian and polar coordinates is depicted in graphic form in Fig. 3. For the stator current and flux linkages, the relationship between the *d*-*q* and *R*-θ coordinates is expressed as follows:

$$\begin{cases} i_d = i_R \cos\theta_i \\ i_q = i_R \sin\theta_i \end{cases}, \tag{6}$$

$$\begin{cases} \lambda_d = \lambda_R \cos\theta_\lambda \\ \lambda_q = \lambda_R \sin\theta_\lambda \end{cases}, \tag{7}$$

where the magnitude and angle are defined as R and θ, respectively. i_R and λ_R are the current and flux magnitudes, and

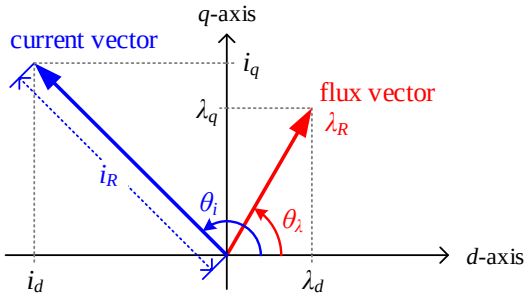

Fig. 3. Relation between Cartesian and polar coordinates.

θ_i and θ_λ are the current and flux angles, respectively.

In R-θ coordinates, the torque equation in (4) can be rewritten as follows by applying (6) and (7).

$$f(i_R,\theta_i)=\frac{3P}{2}\sin(\theta_i-\theta_\lambda)\lambda_R i_R\,. \tag{8}$$

This shows that the torque magnitude is related to the cross product of the current vector and flux vector. In this case, the flux magnitude varies with the current magnitude and the current angle, i.e., $\lambda_R(i_R, \theta_i)$, which should be considered for MTPA operation.

The MTPA equation can be derived from the partial derivative of the torque equation with respect to the current angle as follows:

$$\begin{aligned}\frac{\partial f(i_R,\theta_i)}{\partial\theta_i}&=\frac{3P}{2}i_R\cdot\frac{\partial}{\partial\theta_i}\{\sin(\theta_i-\theta_\lambda)\lambda_R\}\\&=\frac{3P}{2}i_R\{\frac{\partial\lambda_R}{\partial\theta_i}\sin(\theta_i-\theta_\lambda)+\lambda_R(1-\frac{\partial\theta_\lambda}{\partial\theta_i})\cos(\theta_i-\theta_\lambda)\}=0.\end{aligned} \tag{9}$$

Eq. (9) can be further simplified by eliminating $-3P/2\cdot i_R$ as

$$g(i_R,\theta_i)=\lambda_R(\frac{\partial\theta_\lambda}{\partial\theta_i}-1)\cos(\theta_i-\theta_\lambda)-\frac{\partial\lambda_R}{\partial\theta_i}\sin(\theta_i-\theta_\lambda)\,, \tag{10}$$

which is equivalent to (5) in d-q coordinates. The equivalence between (5) and (10) is described in the Appendix.

The MTPA operation can be achieved by solving $g(i_R, \theta_i) = 0$, where the information of flux linkages and its derivatives is required. This reveals that not only the flux magnitude and angle, i.e., λ_R and θ_λ, but also its variations in θ coordinate, i.e., $\partial\theta_\lambda/\partial\theta_i$ and $\partial\lambda_R/\partial\theta_i$, should be considered for MTPA operation. The relation between θ_i and the flux vector can be expressed as follows:

$$\theta_i=h(\lambda_R,\theta_\lambda)=\theta_\lambda+\operatorname{atan}\left\{\lambda_R(\frac{\partial\theta_\lambda}{\partial\theta_i}-1)/\frac{\partial\lambda_R}{\partial\theta_i}\right\}. \tag{11}$$

It can be observed that $h(\lambda_R, \theta_\lambda)$ contains an arctangent function, in which the denominator is $\partial\lambda_R/\partial\theta_i$. Because $\partial\lambda_R/\partial\theta_i$ would be highly fluctuated by flux linkage and its variations, $h(\lambda_R, \theta_\lambda)$ will also be a highly nonlinear.

Fig. 4 shows the contours of the torque and MTPA equation for the motor under test in R-θ coordinates for the positive torque region. The torque equation, $f(i_R, \theta_i)$, monotonically increases with the current magnitude, i_R, as shown in Fig. 4(a). Thus, the torque reference can be tracked by regulating the current magnitude as $T_{e,ref} = f(i_R, \theta_i)$. The torque equation converges asymptotically to $T_{e,ref}$ by applying a closed-loop control structure.

Likewise, the MTPA equation, $g(i_R, \theta_i)$, is a monotonically

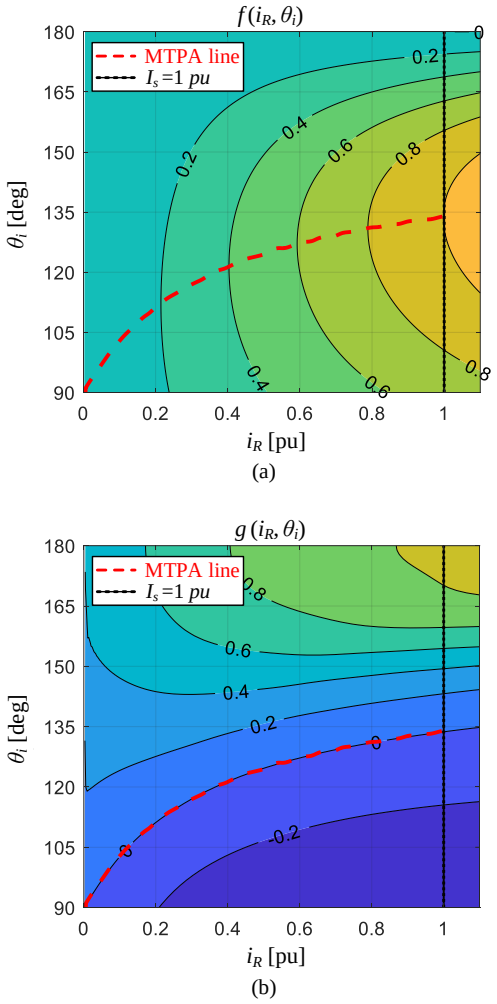

Fig. 4. Contours of torque and MTPA equations with R-θ axes. (a) $f(i_R, \theta_i)$. (b) $g(i_R, \theta_i)$.

increasing function of the current angle, θ_i, as shown in Fig. 4(b). The current angle can be adjusted to maintain the MTPA operation as $g(i_R, \theta_i) = 0$. The MTPA equation converges to 0 with a closed-loop structure owing to its monotonic relationship. In contrast to positive torque conditions, the MTPA equation is a monotonically decreasing function of the current angle under negative torque conditions. With respect to the current angle, the variation of MTPA equation, i.e., $\partial g(i_R, \theta_i)/\partial\theta_i$, has a different direction according to the sign of the torque, which is also related to the sign of the current magnitude.

III. Proposed Dual-Loop Control

Fig. 5 shows the overall block diagram of the proposed dual-loop controller. The current controller is the inner loop of the proposed controller, and the bandwidth of the inner loop is higher than that of the outer loop. The dual-loop controller consists of the current magnitude controller, the current angle controller, and several coordinate transformations, as depicted by the dashed line. The stator currents and current references are converted from R-θ to d-q coordinates or inversely in $R\theta/dq$ and $dq/R\theta$ blocks, which are calculated by trigonometric

This article has been accepted for publication in a future issue of this journal, but has not been fully edited. Content may change prior to final publication. Citation information: DOI 10.1109/TPEL.2021.3120405, IEEE Transactions on Power Electronics

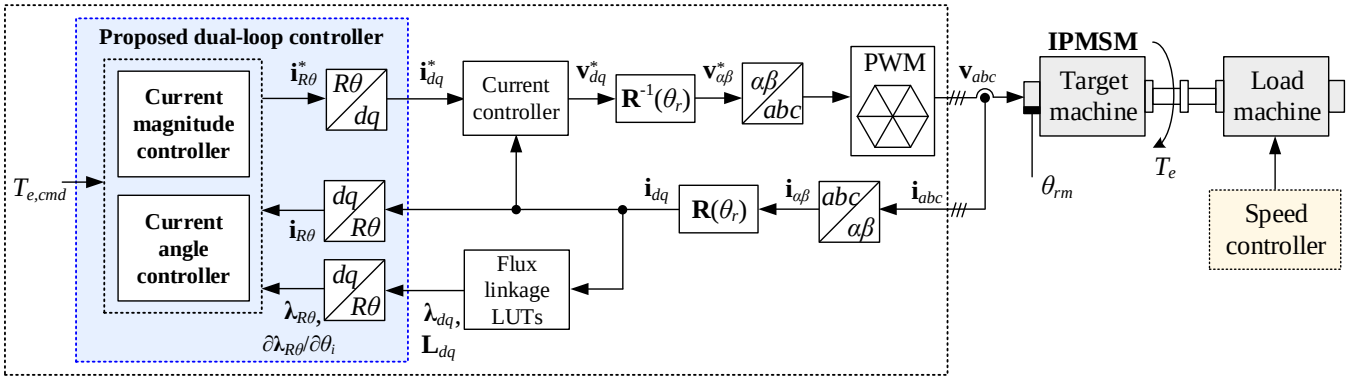

Fig. 5. Overall block diagram of the proposed dual-loop controller.

functions as follows:

$$\begin{cases} i_d^* = i_R^* \cos\theta_i^* \\ i_q^* = i_R^* \sin\theta_i^* \end{cases}, \tag{12}$$

$$\begin{cases} i_R = \sqrt{i_d^2 + i_q^2} \\ \theta_i = \text{atan2}(i_q, i_d) \end{cases}, \tag{13}$$

where atan2(y, x) returns a four-quadrant arctangent of (x, y) in the range of $[-\pi, \pi]$. Likewise, the flux linkages are converted from R-θ to d-q coordinates as follows:

$$\begin{cases} \lambda_R = \sqrt{\lambda_d^2 + \lambda_q^2} \\ \theta_\lambda = \text{atan2}(\lambda_q, \lambda_d) \end{cases}, \tag{14}$$

The proposed controller requires information on the stator flux and dynamic inductance at the operating point. The flux linkages can be identified by applying the stator voltage equations of the IPMSM under steady-state operations. The flux linkage LUTs can be built in advance through experimental tests, where the influence of magnetic saturation and cross-coupling effects are fully considered. [21], [22]. The dynamic inductances can be obtained from the differences between two adjacent points of the flux linkages as follows:

$$L_{dd}(i_d, i_q) = \frac{\lambda_d(i_d + \Delta i_d, i_q) - \lambda_d(i_d, i_q)}{\Delta i_d}, \tag{15}$$

where $L_{dq}(i_d, i_q)$, $L_{qd}(i_d, i_q)$, $L_{qq}(i_d, i_q)$ are calculated in a similar manner.

On behalf of the flux linkage LUTs, estimation algorithms can be adapted to reflect the flux linkage and inductance variations [23]–[27]. The flux linkage variations due to temperature change deteriorate the accuracy of the online MTPA control. Thus, the estimators adequate for the proposed controller can be added to mitigate parameter errors. First, λ_R and θ_λ are estimated by applying the flux observer with $dq/R\theta$ blocks. A hybrid-model based flux observer can be utilized to estimate the flux linkages over a wide speed range [24], [25]. In addition, $\partial\theta_\lambda/\partial\theta_i$ and $\partial\lambda_R/\partial\theta_i$ are required to search the MTPA points in the proposed method. It can be extracted by injecting a high-frequency signal only into the θ coordinate. It can minimize torque variations due to the signal injection because the torque with respect to the current angle is almost zero near MTPA points, i.e., $\partial f(i_R, \theta_i)/\partial\theta_i \approx 0$ [7]. The proposed dual-loop controller can be implemented together with the estimation algorithms as aforementioned. However, this study focuses on the closed dual-loop controller, i.e., the current magnitude and current angle controller itself.

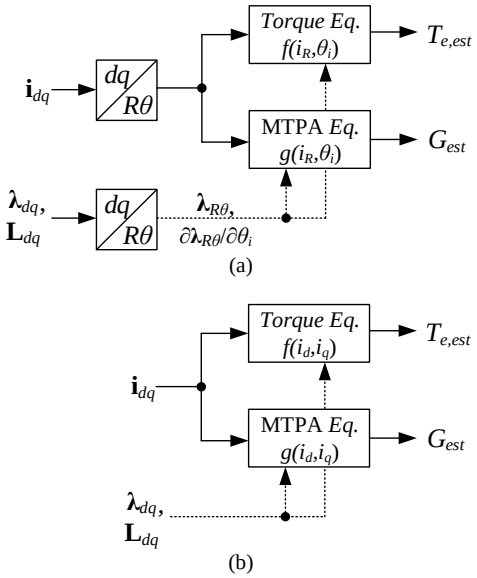

Fig. 6. Implementation of feedback path of the proposed controller. (a) R-θ coordinates, (b) d-q coordinates.

If necessary, the torque and MTPA equations in R-θ coordinates coupled with $dq/R\theta$ blocks can be replaced with the equations in d-q coordinates. Fig. 6(a) shows the feedback path based on R-θ coordinates, where the parameters in d-q coordinates are utilized. In this case, $\partial\lambda_R/\partial\theta_i$ and $\partial\theta_\lambda/\partial\theta_i$ are derived using the chain rule for partial derivatives as follows:

$$\begin{aligned} \frac{\partial\lambda_R}{\partial\theta_i} &= \frac{\partial\lambda_R}{\partial i_d}\frac{\partial i_d}{\partial\theta_i} + \frac{\partial\lambda_R}{\partial i_q}\frac{\partial i_q}{\partial\theta_i} \\ &= \frac{1}{\sqrt{\lambda_d^2 + \lambda_q^2}}\left\{(\lambda_q L_{qq} + \lambda_d L_{dq})i_d - (\lambda_d L_{dd} + \lambda_q L_{qd})i_q\right\} \end{aligned}, \tag{16}$$

$$\begin{aligned} \frac{\partial\theta_\lambda}{\partial\theta_i} &= \frac{\partial\theta_\lambda}{\partial i_d}\frac{\partial i_d}{\partial\theta_i} + \frac{\partial\theta_\lambda}{\partial i_q}\frac{\partial i_q}{\partial\theta_i} \\ &= \frac{1}{\lambda_d^2 + \lambda_q^2}\left\{(\lambda_d L_{qq} - \lambda_q L_{dq})i_d + (\lambda_q L_{dd} - \lambda_d L_{qd})i_q\right\} \end{aligned}. \tag{17}$$

This can be simplified by applying the equations in d-q coordinates, as shown in Fig. 6(b). The flux linkages and dynamic inductances in d-q coordinates would not be changed

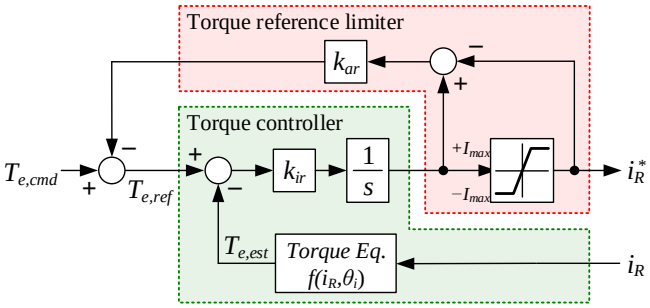

Fig. 7. Block diagram of the proposed current magnitude controller.

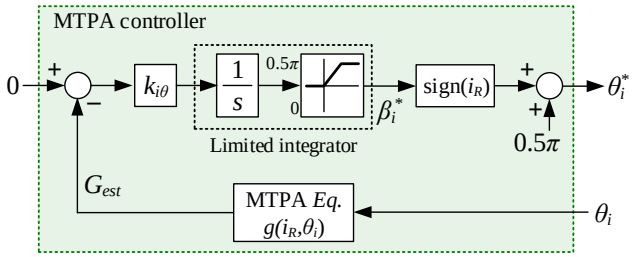

Fig. 8. Block diagram of the proposed current angle controller.

to those in R-θ coordinates.

A. Current Magnitude Control

Fig. 7 shows the block diagram of the proposed current magnitude controller. It consists of a torque controller and a torque reference limiter. In the torque controller, the estimated torque, $T_{e,est}$, is compared with the realizable torque reference, $T_{e,ref}$, where (8) is utilized to calculate $T_{e,est}$. The integral controller is applied to minimize the error between $T_{e,ref}$ and $T_{e,est}$, where the current magnitude reference, i_R^*, is regulated by the feedback loop. Thus, the integral gain of the torque controller, denoted as k_{ir}, determines the bandwidth of the controller. The feedback loop maintains a negative loop gain at both positive and negative torque conditions when the integral gain is set to a positive value: $k_{ir} > 0$, which leads to stable responses.

When the negative torque reference is applied, i_R^* is regulated to a negative value. The negative i_R^* may seem illogical in the physical definition of i_R^*, which indicates the current magnitude. However, it plays a crucial role in maintaining the torque accuracy with the MTPA operation in the regenerative mode, cooperating with the current angle controller described in the next section.

In the torque reference limiter, the absolute magnitude of i_R^*, defined as $|i_R^*|$, is limited to the current limit, I_{max}, which is implemented by an output limiter. I_{max} can be determined by the current rating of the inverter and motor itself and/or the active thermal management strategy [28], [29]. Thus, I_{max} can be adjusted in real-time according to external conditions. When the torque command, $T_{e,cmd}$, exceeds the maximum torque, the output of the integral controller gradually increases and exceeds I_{max}. In this case, $T_{e,ref}$ can be adjusted using an anti-windup algorithm around the limiter. It works based on the difference between the input and output of the limiter to adapt $T_{e,ref}$ within realizable ranges. The dynamics of the torque reference limiter are determined by the anti-windup gain of the torque controller, k_{ar}.

B. Current Angle Control

Fig. 8 shows the block diagram of the proposed current angle controller, i.e., the MTPA controller, where the MTPA equation is solved by a closed-loop controller. The MTPA equation in (10) is applied to extract G_{est}, where G_{est} is the deviation from the MTPA operation. In the MTPA controller, a current beta angle reference, β_i^*, is adjusted to nullify the G_{est}. That is, the MTPA operation can be achieved as G_{est} converges to zero. In this case, β_i^* indicates the angle difference between the current vector and the q-axis. It is regulated by the feedback loop, where the integral gain of the MTPA controller, denoted as $k_{i\theta}$, determines the bandwidth of the current angle controller. Subsequently, β_i^* should be limited within an acceptable range between 0 and 0.5π, where the d-axis current reference always has a negative value.

For the stable operation, the controller should maintain a negative loop gain over the entire operating range. However, the feedback gain at (10) has a different sign according to the direction of the torque. The partial derivative of G_{est} with respect to θ_i, $\partial G_{est}/\partial\theta_i$, has a positive value at the positive torque, i.e., $\partial G_{est}/\partial\theta_i > 0$ for $i_R > 0$. Otherwise, $\partial G_{est}/\partial\theta_i$ has a negative value at the negative torque, i.e., $\partial G_{est}/\partial\theta_i < 0$ for $i_R < 0$. To maintain the negative gain regardless of the operating mode, the current angle reference, θ_i^*, is set to

$$\theta_i^* = sign(i_R)\cdot\beta_i^* + 0.5\pi\,, \tag{18}$$

where θ_i^* is defined in the range of $[0, \pi]$.
As a result, θ_i^* is adjusted within the acceptable range as

$$\begin{cases} 0.5\pi \le \theta_i^* < \pi & (i_R \ge 0) \\ 0 < \theta_i^* \le 0.5\pi & (i_R < 0) \end{cases}. \tag{19}$$

This shows that the current references are located in the 2nd quadrant for positive torque, $i_d^* < 0$ and $i_q^* > 0$. For negative torque, the current references are located in the 3rd quadrant, $i_d^* < 0$ and $i_q^* < 0$, which maintains the stable operation of the IPMSM.

Furthermore, the feedback gain has negligible impact when the current magnitude is close to zero. It has no meaning at β_i^* when $i_R = 0$ because the current references, i_{dq}^*, are set to zero regardless of β_i^*. However, it would deteriorate the transient responses near zero-torque conditions if β_i^* is stuck on an ill point. Thus, β_i^* should converge to zero near zero-torque conditions for stable transitions. Observing (10), because the stator flux near the zero-torque region would be nothing but the flux linkage of the permanent magnet, λ_f, regardless of β_i^*, G_{est} can be approximated as follows:

$$G_{est} \approx \lambda_f \sin(\beta_i^*)\,. \tag{20}$$

Therefore, the proposed current angle controller can regulate β_i^* to null even near the zero-current region. This feature helps the proposed controller to work without jerking in the low-torque region or at torque reversal. However, some distortions such as sensor noise and quantization error can provoke errors near zero current regions. It can be easily implemented by decreasing the upper limit of the limited integrator from 0.5π to null near $i_R = 0$, if necessary.

C. Dynamic Analysis

To analyze the torque dynamics, the variation of $T_{e,est}$ with respect to i_R is derived as a small-signal model, i.e., $\partial T_{e,est}/\partial i_R$. It can be applied to linearize torque dynamics as follows:

$$k_{ir} = \frac{\omega_{cr}}{\dfrac{\partial f(i_R,\theta_i)}{\partial i_R}}, \tag{21}$$

where ω_{cr} means the bandwidth of the torque controller.

In this case, the dynamics of the current controller are assumed to be sufficiently fast compared to those of the torque controller, as mentioned previously. Likewise, the variation of $T_{e,est}$ with respect to θ_i , i.e., $\partial T_{e,est}/\partial \theta_i$, could be derived. However, the effects of $\partial T_{e,est}/\partial \theta_i$ are ignored because the operating point is near the MTPA line at all times by the proposed controller, where $\partial T_{e,est}/\partial \theta_i$ is converged to zero. Thus, the torque dynamics are only related to $\partial T_{e,est}/\partial i_R$, where the derivative terms such as $\partial \lambda_R/\partial i_R$ and $\partial \theta_\lambda/\partial i_R$ are included as follows:

$$\begin{aligned}&\frac{\partial f(i_R,\theta_i)}{\partial i_R}\\ &= \frac{3P}{2}\{(\lambda_R + \frac{\partial \lambda_R}{\partial i_R} i_R)\sin(\theta_i - \theta_\lambda) - \lambda_R i_R \frac{\partial \theta_\lambda}{\partial i_R}\cos(\theta_i - \theta_\lambda)\}.\end{aligned} \tag{22}$$

The signal injection can obtain the terms in R coordinate. However, the injection in the R coordinate provokes torque variations, which are not suitable for torque-control applications. Likewise, the torque reference limiter dynamics are related to $\partial T_{e,est}/\partial i_R$ at the current limit condition.

MTPA dynamics can be linearized by setting $k_{i\theta}$ as

$$k_{i\theta} = \frac{\omega_{c\theta}}{\dfrac{\partial g(i_R,\theta_i)}{\partial \theta_i}}, \tag{23}$$

where $\omega_{c\theta}$ is the bandwidth of the MTPA controller.

However, it requires the second derivative terms $\partial^2\theta_\lambda/\partial\theta_i^2$ and $\partial^2\lambda_R/\partial\theta_i^2$, which makes it challenging to obtain accurate gain normalization in real-time without pretests. Thus, the gains of the proposed controller, i.e., k_{ir}, k_{ar}, and $k_{i\theta}$, are set based on the pretest results and set as constant values. In this case, the burden for updating the controller gains can be saved at the cost of bandwidth accuracy. MTPA dynamics are affected by i_R variations unlike torque dynamics, where the effects of $\partial T_{e,est}/\partial \theta_i$ are not decoupled in the MTPA controller. The bandwidth of MTPA controller is recommended to be higher than that of the torque controller to suppress the overshoot during transients.

Fig. 9(a) shows the derivative of the torque equation to the current magnitude, $\partial f(i_R, \theta_i)/\partial i_R$ on the pu basis. This small-signal gain has a similar value for the MTPA line from zero to rated torque conditions. Thus, the torque dynamics are quite linear when k_{ir} is set to a constant gain. Likewise, the dynamics of torque reference limiter are equal to $\partial f(i_R, \theta_i)/\partial i_R$ at $|i_R| = I_{max}$, where k_{ar} is set as a constant gain. Fig. 9(b) shows the derivative of the MTPA equation to the current angle, $\partial g(i_R, \theta_i)/\partial \theta_i$. The small-signal gain is reduced when the current magnitude is close to 0 pu, e.g., $|i_R| < 0.3$ pu. This means that the MTPA dynamics would be degraded under lower i_R. It can be compensated by variable k_{ir} inversely proportional to i_r. On the other hand, the variation in small-signal gain is relatively small as the current magnitude increases. Thus, $k_{i\theta}$ is set as a constant.

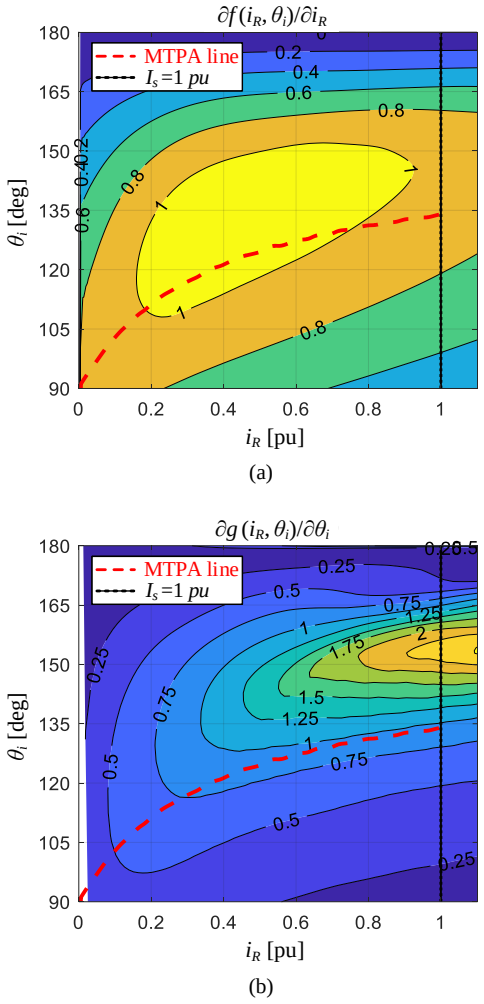

Fig. 9. Contours of torque and MTPA derivatives with R-θ axes. (a) $\partial f(i_R, \theta_i)/\partial i_R$. (b) $\partial g(i_R, \theta_i)/\partial \theta_i$.

IV. Simulation and Experimental Results

A. Simulation Results

A flux-linkage-based high-fidelity IPMSM model [30] was utilized to simulate the actual characteristics of an IPMSM, including cross-coupling and saturation effects, which were constructed using MATLAB/Simulink. The detailed parameters of the IPMSM were extracted by conducting an FEA. The flux linkages and dynamic inductances were obtained by linear interpolation from the flux linkages of the FEA data and the differences between two adjacent points, respectively. The switching and sampling frequencies, f_{sw} and f_{samp}, were set to 10 kHz. The bandwidth of the current regulator was set to $2\pi\cdot250$ rad/s. The gains of the proposed controller, k_{ir}, k_{ar}, and $k_{i\theta}$, were set as constant values, as aforementioned. The torque and MTPA controller bandwidth, ω_{cr} and $\omega_{c\theta}$, were set to $2\pi\cdot25$ rad/s and $2\pi\cdot50$ rad/s, respectively, which were based on the maximum torque condition.

Fig. 10 shows the current reference waveforms at R-θ and d-q coordinates during torque reference transients. The torque

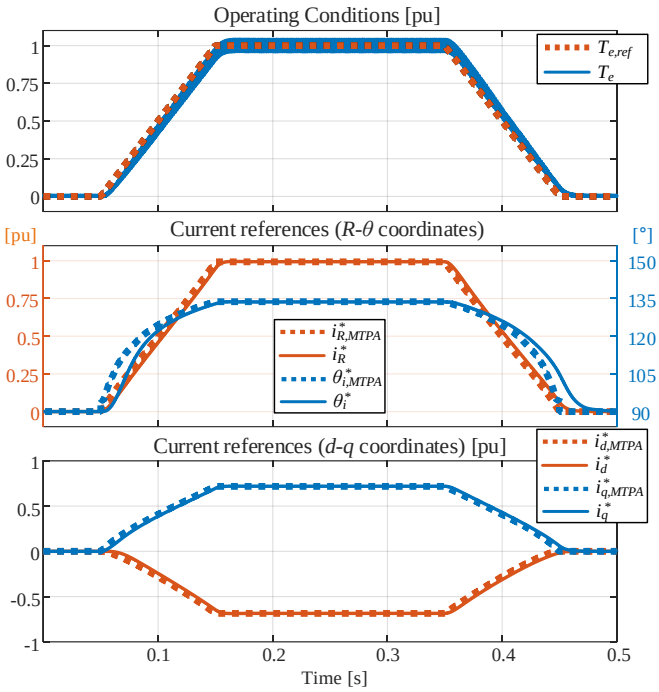

(a)

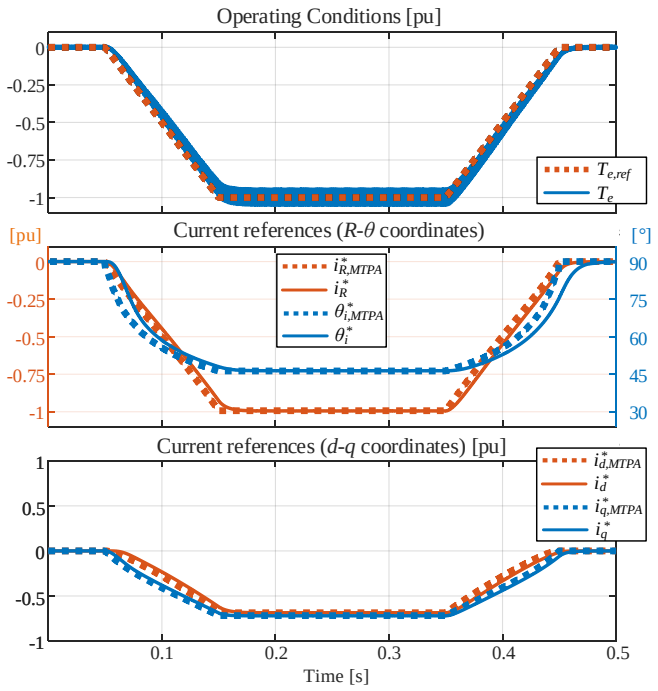

(b)

Fig. 10. Simulation 1: current reference waveforms under torque reference transients at (a) motoring mode and (b) generating mode.

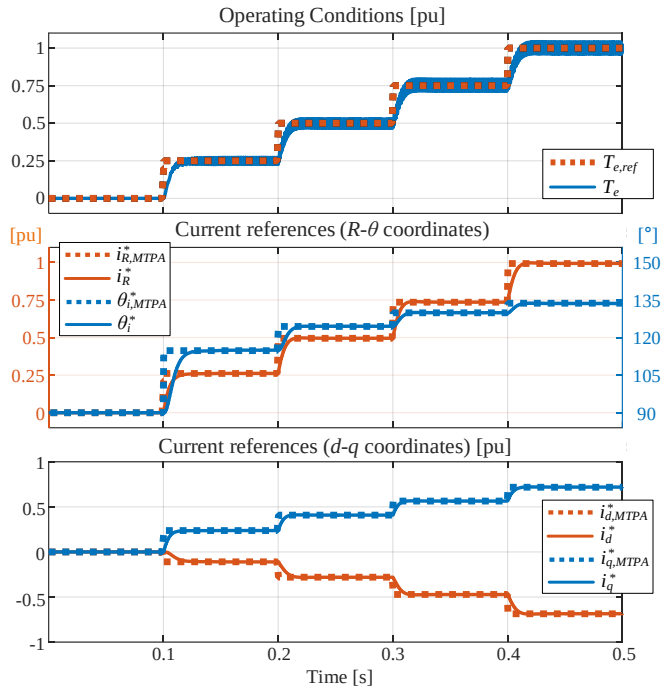

Fig. 11. Simulation 2: current reference waveforms under $T_{e,cmd}$ variations.

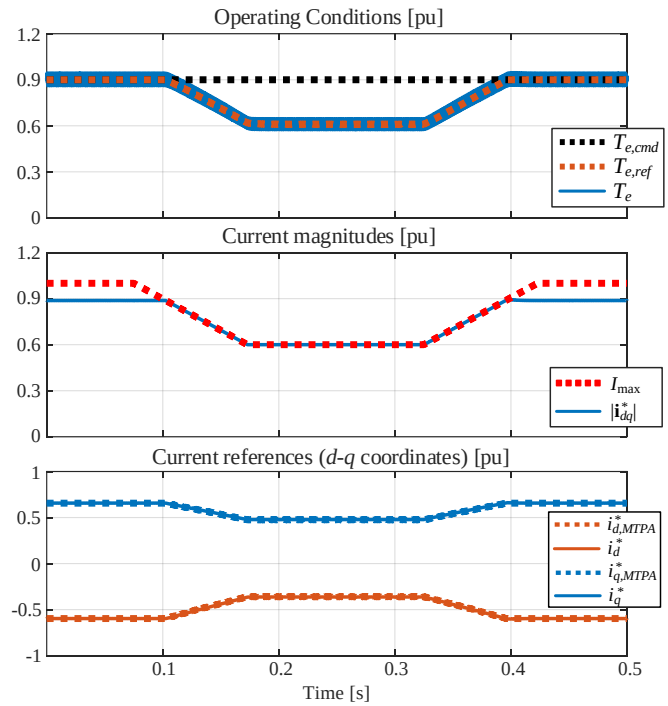

Fig. 12. Simulation 3: torque and current reference waveforms under I_{max} variations.

command varies from zero to full torque and vice versa below the rated speed, where the $T_{e,cmd}$ variation is set to 10 pu/s. The current references based on the proposed method, $\mathbf{i}_{R\theta}{}^* \equiv (i_R{}^*, \theta_i{}^*)$, converge to the MTPA current references, $\mathbf{i}_{R\theta,MTPA}{}^* \equiv (i_{R,MTPA}{}^*, \theta_{i,MTPA}{}^*)$, which shows that both the MTPA operation and torque accuracy are satisfied. In this case, $i_R{}^*$ and $\theta_i{}^*$ are adjusted within a stable range by applying the proposed dual-loop controller. Fig. 10(a) shows ($i_R{}^* \geq 0$) and ($0.5\pi \leq \theta_i{}^* < \pi$) in the motoring mode. Fig. 10(b) shows ($i_R{}^* < 0$) and ($0 < \theta_i{}^* \leq 0.5\pi$) in the generating mode. As a result, the current references, $\mathbf{i}_{dq}{}^* \equiv (i_d{}^*, i_q{}^*)$, trace the MTPA trajectory, $\mathbf{i}_{dq,MTPA}{}^* \equiv (i_{d,MTPA}{}^*, i_{q,MTPA}{}^*)$, even under transient conditions with less calculation burden. In low-torque regions, the MTPA dynamics would be degraded owing to the fixed bandwidth. However, it has scarcely any impact at d-q coordinates and can be adjusted by

changing the controller bandwidth, as mentioned previously.

Fig. 11 shows the current reference waveforms under $T_{e,cmd}$ variations from 0 to 1 pu in steps of 25 % increment every 0.1 s. The proposed method traces the MTPA operating point in R-θ coordinates, $\mathbf{i}_{R\theta,MTPA}^*$, by using the flux linkage information. Thus, $\mathbf{i}_{dq}^*$ and T_e are equal to $\mathbf{i}_{dq,MTPA}^*$ and $T_{e,ref}$, respectively, under steady-state conditions. It shows that T_e traces $T_{e,cmd}$ with no overshoot, where the rising time is determined by the controller's bandwidth.

Fig. 12 shows torque and current reference waveforms, $\mathbf{i}_{dq}^*$ and T_e, under the transition of I_{max} from 1 to 0.6 pu and vice versa where $T_{e,cmd}$ is set to 0.9 pu. The limiting value, I_{max}, can be updated in real-time according to the thermal condition of the inverter and motor as aforementioned. Both torque accuracy and MTPA control can be achieved even when $T_{e,cmd}$ exceeds the maximum available torque due to I_{max}'s suppression as shown in 0.1 s < t < 0.4 s. When $|\mathbf{i}_{dq}^*|$ reaches I_{max}, the anti-windup scheme reduces the current magnitude until the maximum available torque. It shows highly dynamic performance under the rapid variation of I_{max}.

B. Experimental Results

The proposed method was also tested using an experimental test setup. All control algorithms were digitally implemented in the DSP, TMS320F28377D, where the control and system parameters were identical to those in the simulation. The flux linkages are calculated in real-time by linear interpolation of the two-dimensional (2-D) LUTs, which have been constructed by pretests in advance. The dynamic inductances were extracted by the differences between two adjacent points of the flux linkage LUTs in real-time. For comparison, the MTPA operating points were extracted from pretests, which were stored in MTPA LUT, i.e., $\mathbf{i}_{R\theta,MTPA}^*$ and $\mathbf{i}_{dq,MTPA}^*$.

Fig. 13 shows the current waveforms under conditions similar to those in Fig. 10. Likewise, $\mathbf{i}_{R\theta}^*$ is adjusted by the proposed dual-loop controller to satisfy both the MTPA operation and torque accuracy, which is compared with $\mathbf{i}_{R\theta,MTPA}^*$. It shows sufficient transient responses under the rapid change in $T_{e,cmd}$, not only in motoring but also in generating conditions. This means that the proposed dual-loop controller can solve the torque and MTPA equations in real-time. The proposed method maintains the calculation accuracy with more straightforward implementations, which can be adopted to minimize the calculation burden.

Fig 14 shows the current reference waveforms under $T_{e,cmd}$ variations in steps of 20 % increment every 0.1 s, similar to those in Fig. 11. The proposed method generates accurate $\mathbf{i}_{dq}^*$ and T_e under steady-state conditions, matched precisely to $\mathbf{i}_{dq,MTPA}^*$ and $T_{e,ref}$, respectively. It reveals that the proposed method traces the MTPA points at each torque reference where the deviation between $T_{e,ref}$ and $T_{e,est}$ is minimized within a short time, about 10 ms. The torque and MTPA dynamics could be improved by adjusting the controller bandwidth, which can be set according to its application.

Fig. 15 shows the torque and current waveforms under the same conditions as those in Fig. 12. Likewise, it shows that accurate $T_{e,ref}$ and $\mathbf{i}_{dq}^*$ are generated under I_{max} variations. When I_{max} is reduced to 0.6 pu, $T_{e,ref}$ is automatically reduced to 0.6 pu by the torque reference limiter. Thus, the maximum torque under I_{max} could be identified in real-time when i_{dq}^* reaches I_{max}. Both experimental results indicate that the proposed method could fulfill both torque accuracy and MTPA operation even under $T_{e,ref}$ and I_{max} variations.

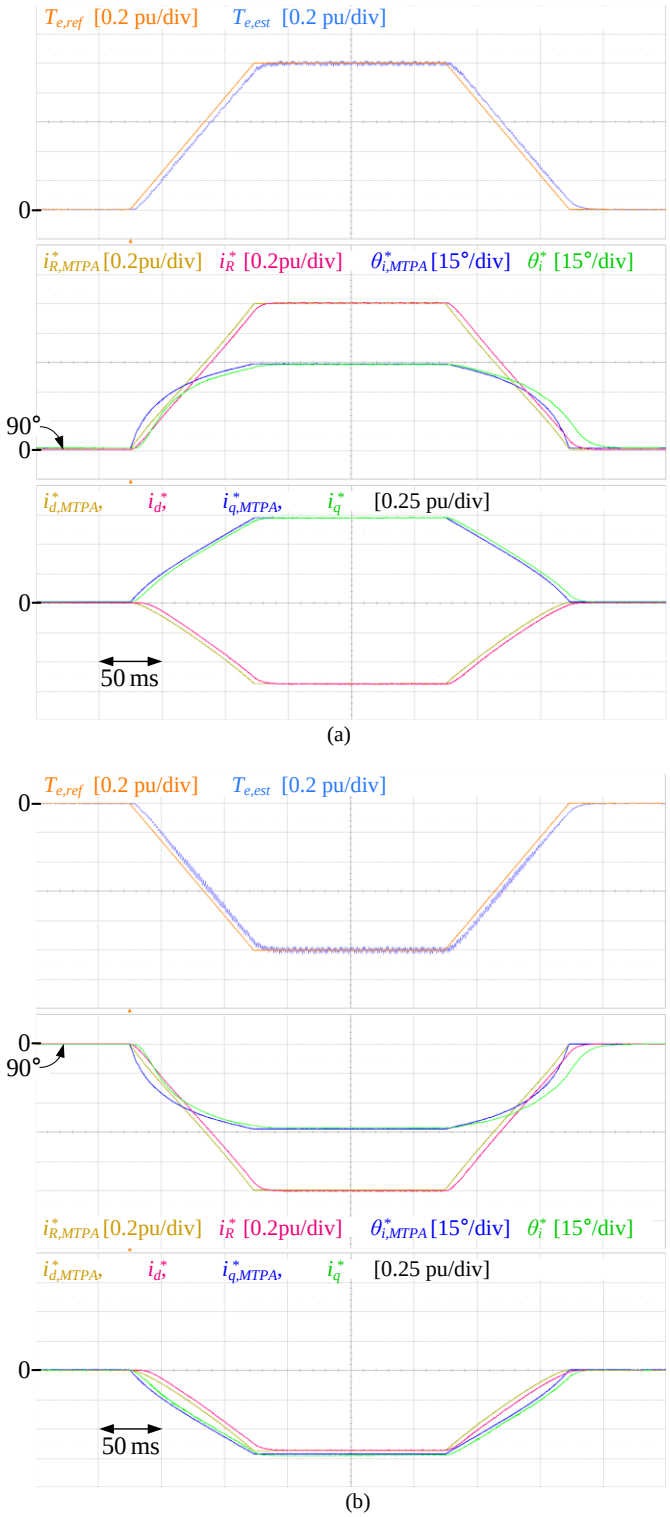

Fig. 13. Experiment 1: current reference waveforms under torque reference transients at (a) motoring mode and (b) generating mode.

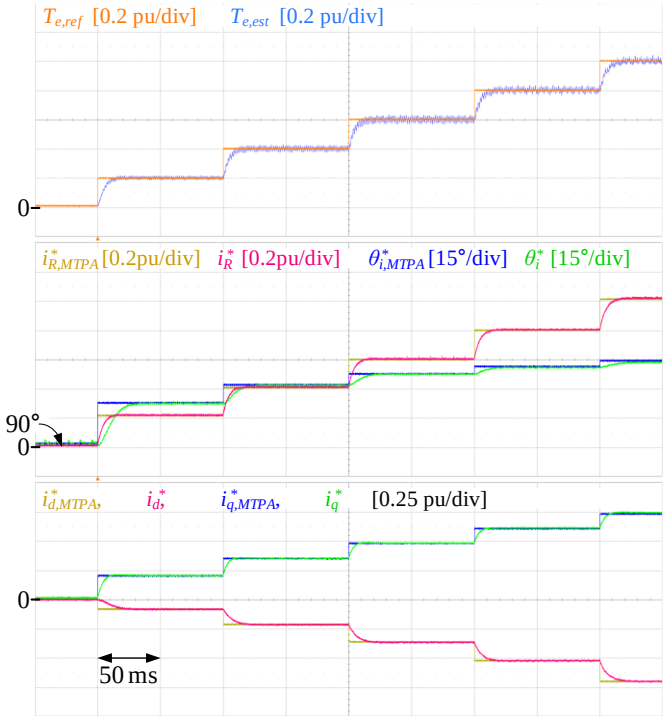

Fig. 14. Experiment 2: current reference waveforms under $T_{e,cmd}$ variations.

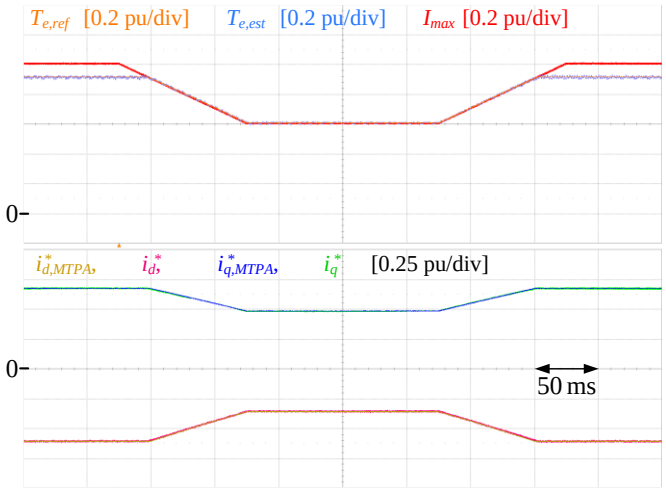

Fig. 15. Experiment 3: torque and current reference waveforms under I_{max} variations.

V. Conclusion

In this paper, the closed dual-loop controller was proposed to satisfy both torque accuracy and MTPA operation. First, the torque and MTPA equations were modeled in polar coordinates, where the current magnitude and current angle correspond roughly to the torque accuracy and MTPA operation, respectively. Thus, the closed-loop controller was utilized to solve the torque and MTPA equations based on its monotonic relationship. In addition, the torque reference limiter was included to restrict the current magnitude to the current limit. The current angle was limited to avoid the stuck of the controller. Owing to the closed-loop structure, the calculation burden could be remarkably reduced while maintaining the calculation accuracy. Finally, the effectiveness of the proposed method was verified by simulation and experimental results using an automotive-grade IPMSM drive system.

Appendix. Checking Equivalenence of MTPA Equations

The MTPA equation in R-θ coordinates in (10) can be rearranged as

$$\lambda_R \frac{\partial \theta_\lambda}{\partial \theta_i}\cos(\theta_i-\theta_\lambda)-\frac{\partial \lambda_R}{\partial \theta_i}\sin(\theta_i-\theta_\lambda)-\lambda_R\cos(\theta_i-\theta_\lambda)=0\,. \quad (24)$$

In this equation, the partial derivative terms $\partial\lambda_R/\partial\theta_i$ and $\partial\theta_\lambda/\partial\theta_i$, are derived as (16) and (17), respectively. Likewise, the trigonometric functions are expressed as

$$\begin{aligned}\sin(\theta_i-\theta_\lambda)&=\sin\theta_i\cos\theta_\lambda-\cos\theta_i\sin\theta_\lambda=\frac{i_q}{i_R}\frac{\lambda_d}{\lambda_R}-\frac{i_d}{i_R}\frac{\lambda_q}{\lambda_R}\\&=\frac{1}{\sqrt{\lambda_d^2+\lambda_q^2}}\frac{1}{\sqrt{i_d^2+i_q^2}}(\lambda_d i_q-\lambda_q i_d)\end{aligned}, \quad (25)$$

$$\begin{aligned}\cos(\theta_i-\theta_\lambda)&=\cos\theta_i\cos\theta_\lambda+\sin\theta_i\sin\theta_\lambda=\frac{i_d}{i_R}\frac{\lambda_d}{\lambda_R}+\frac{i_q}{i_R}\frac{\lambda_q}{\lambda_R}\\&=\frac{1}{\sqrt{\lambda_d^2+\lambda_q^2}}\frac{1}{\sqrt{i_d^2+i_q^2}}(\lambda_d i_d+\lambda_q i_q)\end{aligned}. \quad (26)$$

The MTPA equation in R-θ coordinates can be expressed by substituting the terms in d-q coordinates. Consequently, the MTPA equation in d-q coordinates can be derived as follows:

$$\frac{1}{\sqrt{i_d^2+i_q^2}}\{(L_{dd}i_q^2-(L_{dq}+L_{qd})i_d i_q+L_{qq}i_d^2)-(\lambda_d i_d+\lambda_q i_q)\}=0\,. \quad (27)$$

References

[1] B. Stumberger, G. Stumberger, D. Dolinar, A. Hamler, and M. Trlep, "Evaluation of saturation and cross-magnetization effects in interior permanent-magnet synchronous motor," *IEEE Trans. Ind. Appl.*, vol. 39, no. 5, pp. 1264–1271, Sep./Oct. 2003.

[2] B.-H. Bae, N. Patel, S. Schulz, and S.-K. Sul, "New field weakening technique for high saliency interior permanent magnet motor," *in Conf. Rec. IEEE IAS Annu. Meeting*, 2003, vol. 2, pp. 898–905.

[3] Y.-S. Kim and S.-K. Sul, "Torque Control Strategy of an IPMSM Considering the Flux Variation of the Permanent Magnet," in *Conf. Rec. IEEE IAS Annu. Meeting (IAS 2007)*, 2007, pp. 1301–1307.

[4] Y. Miao, H. Ge, M. Preindl, J. Ye, B. Cheng, and A. Emadi, "MTPA Fitting and Torque Estimation Technique Based on a New Flux-Linkage Model for Interior-Permanent-Magnet Synchronous Machines," *IEEE Trans. Ind. Appl.*, vol. 53, no. 6, pp. 5451-5460, Nov./Dec. 2017.

[5] A. Rabiei, T. Thiringer, M. Alatalo, and E. A. Grunditz, "Improved Maximum-Torque-Per-Ampere Algorithm Accounting for Core Saturation, Cross-Coupling Effect, and Temperature for a PMSM Intended for Vehicular Applications," *IEEE Trans. Transp. Electrif.*, vol. 2, no. 2, pp. 150–159, Jun. 2016.

[6] S. Bolognani, R. Petrella, A. Prearo, and L. Sgarbossa, "Automatic Tracking of MTPA Trajectory in IPM Motor Drives Based on AC Current Injection," *IEEE Trans. Ind. Appl.*, vol. 47, no. 1, pp. 105–114, Jan./Feb. 2011.

[7] S. Kim, Y.-D. Yoon, S.-K. Sul, and K. Ide, "Maximum Torque per Ampere (MTPA) Control of an IPM Machine Based on Signal Injection Considering Inductance Saturation," *IEEE Trans. Power Electron.*, vol. 28, no. 1, pp. 488–497, Jan. 2013.

[8] R. Antonello, M. Carraro, and M. Zigliotto, "Maximum-Torque-Per-Ampere Operation of Anisotropic Synchronous Permanent-Magnet Motors Based on Extremum Seeking Control," *IEEE Trans. Ind. Electron.*, vol. 61, no. 9, pp. 5086–5093, Sep. 2014.

[9] Y. A.-R. I. Mohamed and T. K. Lee, "Adaptive Self-Tuning MTPA Vector Controller for IPMSM Drive System," *IEEE Trans. Energy Convers.*, vol. 21, no. 3, pp. 636–644, Sep. 2006.

[10] Q. Liu and K. Hameyer, "High-Performance Adaptive Torque Control for an IPMSM With Real-Time MTPA Operation," *IEEE Trans. Energy Convers.*, vol. 32, no. 2, pp. 571–581, Jun. 2017.

[11] K. Liu, Q. Zhang, J. Chen, Z. Q. Zhu, and J. Zhang, "Online Multiparameter Estimation of Nonsalient-Pole PM Synchronous Machines With Temperature Variation Tracking," *IEEE Trans. Ind. Electron.*, vol. 58, no. 5, pp. 1776–1788, May 2011.

[12] T. Sun, J. Wang, and M. Koc, "On Accuracy of Virtual Signal Injection based MTPA Operation of Interior Permanent Magnet Synchronous Machine Drives," *IEEE Trans. Power Electron.*, vol. 32, no. 9, pp. 7405–7408, Sep. 2017.

[13] S.-Y. Jung, J. Hong, and K. Nam, "Current Minimizing Torque Control of the IPMSM Using Ferrari's Method," *IEEE Trans. Power Electron.*, vol. 28, no. 12, pp. 5603–5617, Dec. 2013.

[14] Y.-S. Jeong, S.-K. Sul, S. Hiti, and K. M. Rahman, "Online Minimum-Copper-Loss Control of an Interior Permanent-Magnet Synchronous Machine for Automotive Applications," *IEEE Trans. Ind. Appl.*, vol. 42, no. 5, pp. 1222–1229, Sep. /Oct. 2006.

[15] H.-S. Kim, Y. Lee, S.-K. Sul, J. Yu, and J. Oh, "Online MTPA Control of IPMSM for Automotive Applications Based on Robust Numerical Optimization Technique," *IEEE Trans. Ind. Appl.*, vol. 55, no. 4, pp. 3737–3746, Jul./Aug. 2019.

[16] A. Varatharajan, G. Pellegrino and E. Armando, "Direct Flux Vector Control of Synchronous Motor Drives: A Small-Signal Model for Optimal Reference Generation," *IEEE Trans. Power Electron.*, vol. 36, no. 9, pp. 10526-10535, Sep. 2021.

[17] A. Varatharajan, G. Pellegrino and E. G. Armando, "Direct Flux Vector Control of Synchronous Motor Drives: Accurate Decoupled Control with Online Adaptive MTPA and MTPV Evaluation," *IEEE Trans. Ind. Electron.*, to be published, doi: 10.1109/TIE.2021.3060665.

[18] H.-S. Kim, and S.-K. Sul, "Real-time Torque Control of IPMSM under Flux Variations," *IEEE J. Emerg. Sel. Top. Power Electron.*, to be published, doi: 10.1109/JESTPE.2020.3032463.

[19] H.-S. Kim, and S.-K. Sul, "Online MTPA Operation Based on Dual-Loop Control in Polar Coordinates," in *2019 10th International Conference on Power Electronics and ECCE Asia (ICPE-ECCE Asia)*, 2019, pp. 2936–2941.

[20] N. Bianchi and S. Bolognani, "Magnetic models of saturated interior permanent magnet motors based on finite element analysis," *in Conf. Rec. IEEE IAS Annu. Meeting (IAS 1998)*, 1998, vol. 1, pp. 27–34.

[21] D. Hu, Y.M. Alsmadi, and L. Xu, "High-fidelity nonlinear IPM modeling based on measured stator winding flux linkage," *IEEE Trans. Ind. Appl.*, vol. 51, no. 4, pp. 3012–3019, Jul./Aug. 2015.

[22] J. Lee, Y.-C. Kwon and S.-K. Sul, "Identification of IPMSM Flux-Linkage Map for High-Accuracy Simulation of IPMSM Drives," *IEEE Trans. Power Electron.*, vol. 36, no. 12, pp. 14257-14266, Dec. 2021.

[23] Y.-S. Jeong and J.-Y. Lee, "Adaptive flux observer with on-line inductance estimation of an interior PM synchronous machine considering magnetic saturation," *J. Power Electron.*, vol. 9, no. 2, pp. 188–197, Mar. 2009.

[24] H.-S. Kim, S.-K. Sul, H. Yoo, and J. Oh, "Distortion-Minimizing Flux Observer for IPMSM Based on Frequency-Adaptive Observers," *IEEE Trans. Power Electron.*, vol. 35, no. 2, pp. 2077-2087, Feb. 2020.

[25] J. Yoo, H.-S. Kim, and S.-K. Sul, "Design of Frequency-Adaptive Flux Observer in PMSM Drives Robust to Discretization Error," *IEEE Trans. Ind. Electron.*, to be published, doi: 10.1109/TIE.2021.3075854.

[26] W. Xu and R. D. Lorenz, "High-Frequency Injection-Based Stator Flux Linkage and Torque Estimation for DB-DTFC Implementation on IPMSMs Considering Cross-Saturation Effects," *IEEE Trans. Ind. Appl.*, vol. 50, no. 6, pp. 3805–3815, Nov./Dec. 2014.

[27] S. Kim and S.-K. Sul, "High Performance Position Sensorless Control Using Rotating Voltage Signal Injection in IPMSM," in *Proc. Eur. Conf. Power Electron. Appl. (EPE 2011)*, 2011, pp. 1–10.

[28] S.-K. Sul, *Control of Electric Machine Drive Systems*. NJ:Wiley, 2011.

[29] J. Lemmens, P. Vanassche, and J. Driesen, "Optimal control of traction motor drives under electrothermal constraints," *IEEE J. Emerg. Sel. Topics Power Electron.*, vol. 2, no. 2, pp. 249–263, Jun. 2014.

[30] X. Chen, J. Wang, B. Sen, P. Lazari, and T. Sun, "A High-Fidelity and Computationally Efficient Model for Interior Permanent-Magnet Machines Considering the Magnetic Saturation, Spatial Harmonics, and Iron Loss Effect," *IEEE Trans. Ind. Electron.*, vol. 62, no. 7, pp. 4044–4055, Jul. 2015.